Ultimate Black Hole Recoil: What is the Maximum High-Energy Collision Kick?

James Healy and Carlos O. Lousto
Center for Computational Relativity and Gravitation (CCRG), School of Mathematical Sciences, Rochester Institute of Technology, 85 Lomb Memorial Drive, Rochester, New York 14623, USA

(Received 30 December 2022; accepted 13 July 2023; published 18 August 2023)

We performed a series of 1381 full numerical simulations of high energy collision of black holes to search for the maximum recoil velocity after their merger. We consider equal mass binaries with opposite spins pointing along their orbital plane and perform a search of spin orientations, impact parameters, and initial linear momenta to find the maximum recoil for a given spin magnitude s. This spin sequence for $s = 0.4, 0.7, 0.8, 0.85, 0.9$ is then extrapolated to the extreme case, $s = 1$, to obtain an estimated maximum recoil velocity of $28,562 \pm 342$ km/s, thus approximately bounded by 10% of the speed of light.

DOI: 10.1103/PhysRevLett.131.071401

Introduction.—Ever since the discovery through full numerical simulations [1,2] that the merger of binary black holes may lead to large (astrophysically speaking) gravitational recoil velocities, a fascinating search for such events in nature takes place [3,4]. Since the first modeling of large recoils [5], it was clear that the spins of the black holes played a crucial role in their merger remnant reaching a speed up to several thousand kilometers per second. Next, a configuration was found [6] that maximized the recoil nearing 5000 km/s. This configuration combined the opposite spins of [5] that maximized asymmetry with the hang-up effect [7] that maximized radiation. All those configurations assumed negligible eccentricities at the time of merger, when most of the asymmetric radiation takes place. While this is the most plausible astrophysical scenario, new gravitational wave observations show the potential for large residual eccentricity in some events [8].

Here, we will explore the extreme scenario of high energy collisions of black holes, in the realm of high-energy colliders, to discover the fundamental laws of nature [9,10], with applications to the gauge-gravity duality, holography [11], primordial black hole collisions in the early Universe [12–14], and as tests of the radiation bounds theorems and cosmic censorship conjecture in general relativity [15–17]. The growth of structure seeded by primordial black holes has been studied in [18], and the effects of gravitational-wave recoil on the dynamics and growth of supermassive black holes has been studied in [19]. While the scenario of supermassive rotating black holes potentially accelerating orbiting black holes to high energies was discussed in [20].

This high energy collision of black holes scenario was studied in [21] to compute the maximum energy radiated by equal mass, nonspinning black holes in an ultrarelativistic head-on collision. This first study was then followed up by the claim that the spin effects did not matter for these collisions in [22]. In [23] we then revisited the head-on scenario using new initial data [24] with low spurious initial radiation content that allows for more accurate estimates of the maximum energy radiated placing it at about 13%. Non-head-on high energy collisions have also been studied in [25], and in notable analytic detail in [26]. Some of the early reviews on the subject are [9,10], and more up-to-date ones are [27–29].

Here, we extend those studies with much larger numerical simulations set by directly solving numerically the general relativity field equations in supercomputers, and by focusing on the computation of the maximum achievable gravitational recoil from grazing, high energy collisions of binary black holes, where the holes' spin orientation and magnitude play a crucial role.

Numerical techniques.—The full numerical simulations were performed using the LazEv code [30] implementation of the moving puncture approach [31]. We use the general relativistic BSSNOK formalism of evolutions systems [32–34]. The LazEv code uses the Cactus [35]–Carpet [36]–EinsteinToolkit [37,38] infrastructure. The Carpet mesh refinement driver provides a "moving boxes" style of mesh refinement. To compute the numerical (Bowen-York) initial data, we use the TwoPunctures [39] code. We use AHFinderDirect [40] to locate apparent horizons and measure the magnitude of the horizon spin S_H, using the *isolated horizon* algorithm as implemented in Ref. [41]. We measure radiated energy, linear momentum, and angular momentum, in terms of the radiative Weyl scalar ψ_4, using the formulas provided in Refs. [42,43]. As described in Ref. [44], we use the Teukolsky equation to analytically extrapolate expressions for $R\psi_4$ from a finite observer location ($R_{\rm obs} > 100M$) to infinity ($\mathcal{I}^+$).

One can hypothesize on asymmetry properties that one can search for the maximum recoil within a family of equal mass, opposite spins on the orbital plane configurations, as displayed in Fig. 1. The compromise with maximizing the energy radiated via the hang-up effect [7] that we needed to

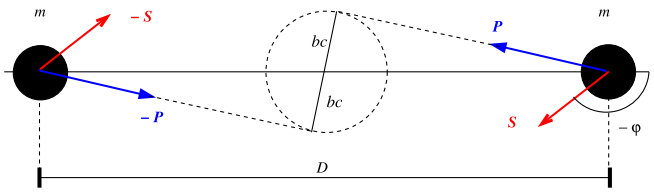

FIG. 1. Maximum high energy collision kicks binary black hole initial configurations. On the orbital plane equal mass m black holes with opposing spin $\vec{S}$ and momentum $\vec{P}$ with critical impact parameter b_c and starting separation $D = 50M$.

find the maximum recoil for quasicircular orbits in [6] is replaced here by the determination of the critical impact parameter b_c separating merger from scattering of the holes. Besides, a certain independence of the energy radiated with the spin of the holes is displayed in Ref. [22].

This Fig. 1 configuration has been studied earlier in [45,46] leading to a wide range of maximum velocity estimates of 10 000 km/s and 15 000 km/s from simulations to potential extrapolations up to 45 000 km/s. Here, we will study this problem in detail with our new set of specially designed simulations to explicitly model the problem in terms of the Bowen-York initial momentum of the holes γv, impact parameter b, and spin, $\vec{s} = \vec{S}_H/m_H^2$ (where $m_H = m_{1,2}$ is the horizon mass of each hole), i.e., a four dimensional parameter search.

Simulations' results.—Our simulations families consist of a choice of an initial (Bowen-York) data spin magnitude, here $s = 0.4$, 0.7, 0.8, 0.85, 0.9, and for each of them an initial momentum per irreducible mass γv, and impact parameter bM, as measured at the initial separation of the holes $D = 50M$ (with $M = m_1 + m_2$ the addition of the horizon masses of the system). We then vary the orientation of the spins pointing on the orbital plane by an angle φ with respect to the line initially joining the black holes. This allows us to model the leading φ dependence of the recoil velocity as a $\cos\varphi$ [47]. In practice one needs about

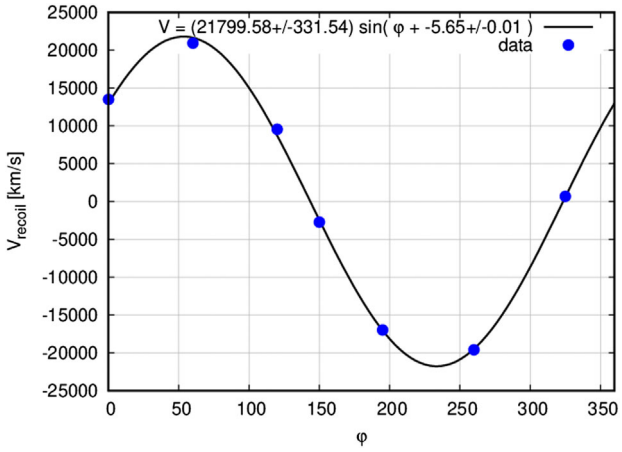

FIG. 2. A series of simulations versus φ orientation of the spin for $b = 2.38$, $s = 0.85$, $\gamma v = 0.874$.

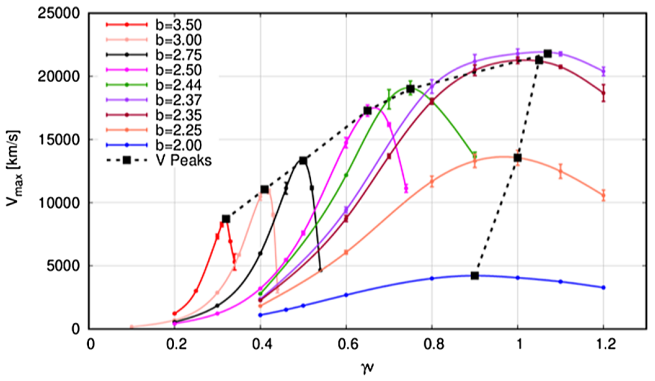

FIG. 3. A series of simulations versus γv and b to search for $V_{\rm max}$ for the spin $s = 0.80$ case.

four to seven simulations to fit this dependence and determine the amplitude of the curve leading to the maximum recoil for this configuration, as for instance displayed in Fig. 2.

To compute recoil velocities from these waveforms in the time domain, we subtract, at the postprocessing stage, the initial burst of spurious radiation. This Bowen-York initial data radiation content reaches earlier the fiducial observer than its more physical components, and thus can be simply excised. The effects of this spurious radiating is, nevertheless, relatively much smaller on the recoil velocities than it is on the radiated energy. For instance, for a case closest to maximum kick $(s = 0.9, b = 2.38, \gamma v = 1.1)$ we get a kick of about 22 700 km/s total, with the spurious burst contributing around 25 km/s. While for the energy radiated, the spurious burst contributes approximately 5% $(0.018/0.336)M$.

The next step in the search for the maximum recoil is to find the peak velocities in the γv and b parameter space. This is achieved as displayed in Fig. 3.

This search process of the impact parameter b to find the value $b_{\rm max}$ leading to the largest recoil velocity is then repeated for each spin value. Figure 4 displays this search

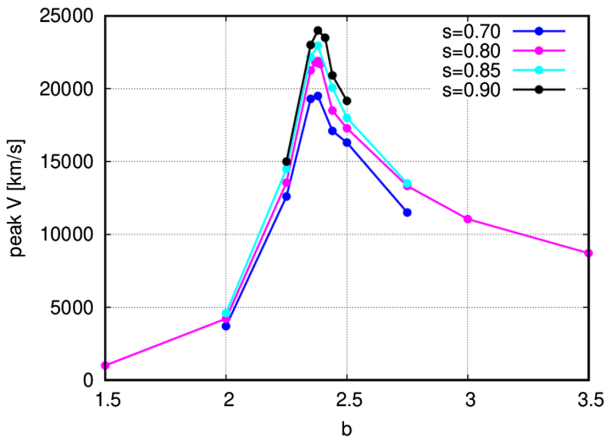

FIG. 4. Maximum recoil velocity for different impact parameters b. For all the high spins studied here this peaks at $b \approx 2.38$.

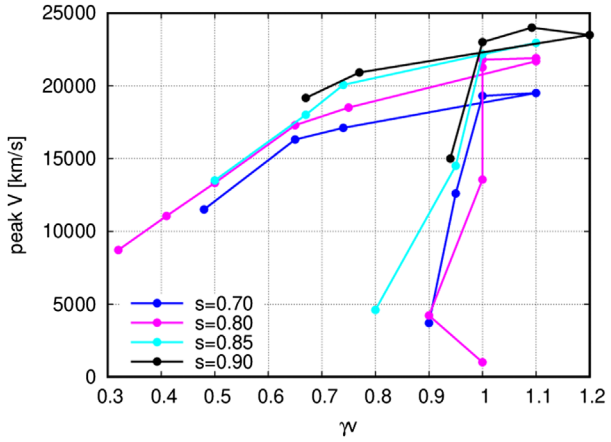

FIG. 5. Display of peak velocity vs γv and spin for merging holes.

for each of the spin magnitudes we considered here. In practice, the $b_{\max}$ corresponds closely to the critical value of the impact parameter b_c separating the direct merger from the scattering of the holes.

A similar analysis can be done by varying the initial velocity v, or rather the linear momentum per irreducible mass of the holes, $\gamma v = P/m_{\rm irr}$, with $\gamma = (1-v^2)^{-1/2}$, the Lorentz factor, and $A_H = 16\pi m_{\rm irr}^2$ the measured horizon area. As displayed in Fig. 5 those curves display the same feature of maximizing the recoil velocity for values about the critical momentum separating the direct merger from scattering of the holes. The return loop of the curves around its maximum represents an overshot of the impact parameter compensated by the lowering of the initial velocity to warrant merger instead of scattering.

The explicit dependence on both parameters, b and γv is displayed in Fig. 6 as a heat map for each of the spin magnitudes $s = 0.7, 0.8, 0.85, 0.9$.

The final results of the maximum recoil velocities for each s and the corresponding relaxed (at around $t = 30M$) spin magnitude $|s_r|$, are summarized in Table I and in Fig. 7, where we display the error bars of each point and fit

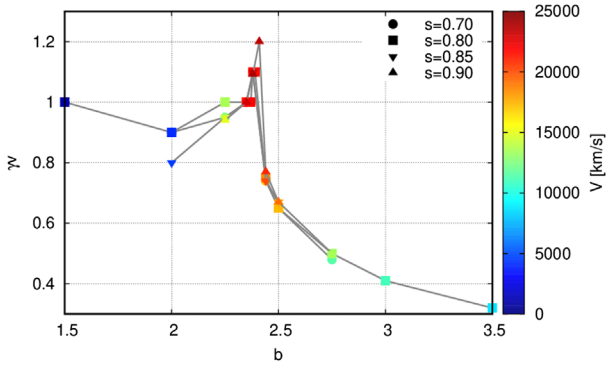

FIG. 6. Maximum recoil velocity for different initial momenta parameters γv and impact parameters b as a color map.

to a quadratic dependence fit on s_r to extrapolate to the ultimate recoil velocity finding $28,562 \pm 342$ km/s for the extremely spinning, $s_r = 1$, binary black holes case. We also display for comparison with the extrapolated to infinite resolution values (in blue) used for the fit, the $n100$ low resolution results (in red), used for the parameter searches.

Note also that in Table I we provide the number of runs (simulations) we performed in the three-dimensional search $(\varphi, b, \gamma v)$ of the maximum recoil for a given spin s. In the case of $s = 0.4$, to simplify the search, and in the light of the previous results with the higher spin cases (as seen in Figs. 4 and 6) we assumed $b = 2.38$, hence the lower number of simulations needed.

For the majority of the simulations, for spins of $s = 0.4$ to $s = 0.85$, we use a grid, labeled as $n100$, with ten levels of refinement, the coarsest of which has resolution of $4M$ and outer boundary of $r = 400M$, with each successive grid with twice the resolution. If we label the coarsest grid $n = 0$, and the finest grid $n = 9$, the resolution on a given level is $M/2^{(n-2)}$. The wave zone is $n = 2$ with a resolution of $M/1$ and boundary out to $r = 125M$. The finest grid has a resolution of $M/128$ with a size of $0.5M$ centered around each black hole. The spin $s = 0.9$ case has an additional refinement level around each black hole with resolution $M/256$ and a radius of $r = 0.3M$.

To evaluate the finite difference errors and extrapolation of our simulations, we have performed three simulation sets with increasing global resolutions by factors of 1.2 ($n120$, $n144$) with respect to our base resolution, $n100$, for the peak velocity cases with $b = 2.38$, $(\gamma v)_{\max}$, and four $\varphi = 0°$, 60°, 120°, 150° degrees for each of the spins $s = 0.40, 0.70, 0.80, 0.85, 0.90$. The resulting measured recoil velocities are given in Table I. Extrapolation to infinite resolution leads to $V^{\infty}_{\max}$ values representing about a 3% increase from the $n100$ results. The third order convergence rate found for the net recoil (computed as

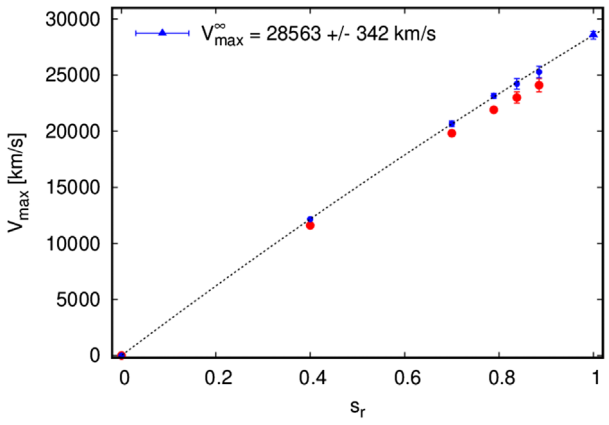

FIG. 7. Maximum recoil velocity versus the settled spins value s_r and its extrapolation to maximal spin $s_r = 1$. (Blue points are extrapolation to infinite resolution, red points are the $n100$ low resolution results).

TABLE I. All simulations have equal mass $m_1 = m_2$ black holes, and are initially placed at $x_{1,2} = \pm 25M$. The relaxed spin magnitudes $|s_r|$ are used for the final fit. Measured maximal recoil velocities and its extrapolation (order) to infinite resolution are given on the right panel.

Number of runs	$\pm s$	$\lvert s_r\rvert$	$b_{\max}$	$(\gamma v)_{\max}$	$V_{\max}^{n100}$ (km/s)	$V_{\max}^{n120}$ (km/s)	$V_{\max}^{n144}$ (km/s)	$V_{\max}^{\infty}$ (km/s)	Order
72	0.40	0.400	2.38	1.20	$11\,637 \pm 67$	$11\,827 \pm 67$	$11\,944 \pm 64$	$12\,133 \pm 189$	2.7
233	0.70	0.699	2.38	1.10	$19\,832 \pm 267$	$20\,163 \pm 267$	$20\,360 \pm 262$	$20\,649 \pm 289$	2.9
472	0.80	0.789	2.38	1.10	$22\,212 \pm 228$	$22\,583 \pm 226$	$22\,800 \pm 217$	$23\,104 \pm 304$	3.0
305	0.85	0.838	2.38	1.10	$23\,291 \pm 514$	$23\,666 \pm 486$	$23\,892 \pm 482$	$24\,231 \pm 339$	2.8
299	0.90	0.885	2.38	1.09	$24\,172 \pm 579$	$24\,609 \pm 565$	$24\,870 \pm 552$	$25\,256 \pm 386$	2.8

large differences of anisotropic radiation), is what one expects from the fourth Runge-Kutta time integrator used by our code.

As a further check of our numerical accuracy, we have recalculated a set of cases for the spin 0.8 and 0.85 with the extra refinement level and increased grid sizes as we used for the spin 0.9 runs. We then recalculated the series that gives a maximum value for spin 0.8 of $21\,802 \pm 191$ km/s. Compared to the original grid computation of $21\,903 \pm 213$ km/s, this leads to a difference of 101 km/s or 0.46%.

Conclusions.—In Fig. 8 we display the spectrum of radiated energy by adding the leading $(\ell = 2, m = 0, \pm 2)$ modes for one of the peak recoil cases ($b = 2.38$, $s = 0.85$, $\gamma v = 1.1$) for different orientation angles φ of the spin. We observe a bulge at low frequencies, corresponding to the initial data content and "bremsstrahlunglike" radiation of the holes approaching each other from $D = 50M$ and that the different spin orientations do not produce notable differences in this part of the spectrum. Meanwhile, at higher frequencies (by an order of magnitude), corresponding to when the holes reach the critical separation $2b_c M = 4.76M$ and then subsequently merge, the spectrum shows a strong dependence on the spin orientations.

To summarize, we have been able to provide an accurate estimate of the ultimate recoil, product of the high energy collision of two black holes. In order to perform the four dimensional search (momentum γv, impact parameter b, spin orientation φ, and magnitude s) we performed 1381 simulations in search for the critical b_c marginally leading to merger and the corresponding value of $\gamma_{\max}$ that maximized the recoil all as a function of φ for each s. Extrapolation to extreme spins (as shown in Fig. 7) have led us to estimate the value of $28\,562 \pm 342$ km/s for the ultimate recoil, placing thus a bound for it of below 10% the speed of light.

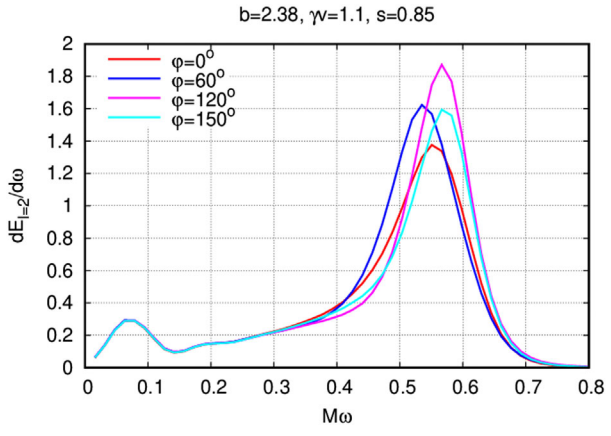

FIG. 8. The spectrum of the ($\ell = 2$ modes) energy radiated $dE_{\ell=2}/d\omega$ by a representative set of simulations (with $b = 2.38$, $s = 0.85$, $\gamma v = 1.1$) for different orientation angles φ of the spin.

We thus note here the crucial relevance of the holes' spin magnitude and orientation in the determination of the high energy collision kicks. In a follow-up paper [48] we plan to study in detail also the role of the spins in the determination of the absolute maximum energy and angular momentum radiated by such systems.

Figures 4 and 6 display a cusplike dependence with the impact parameter b around its $b_{\max}$ value that is reminiscent of critical behavior separating direct merger from scattering of the holes. Critical behavior was discussed in detail in Ref. [26] in the context of the energy radiated by this ultrarelativistic black hole encounters, identifying impacts parameters for direct merger b^* and unbound scattering b_{scat}. Here, we observe this kind of behavior regarding the approach to the maximum radiated *linear* momentum as the impact parameter reaches its critical value $b_{\max}$ and $\gamma v_{\max}$, analogous to the critical temperature and pressure in a liquid-gas system. The intermediate impact parameter region between direct merger and direct scattering acts in a way to match those values of the recoil velocity in a continuous way, thus conforming the equivalent of a second order phase transition (in the Ehrenfest classification). Further studies to verify critical behavior and to obtain critical exponents, as to verify to what extent one can speak of universality, order parameters, and scaling properties in this context, is certainly of interest and deserves follow-up research, preferably with semianalytic methods [48] since 3D critical phenomena remains extremely challenging with full numerical relativity.

The authors gratefully acknowledge the National Science Foundation (NSF) for financial support from Grants No. PHY-1912632 and No. PHY-2207920. Computational resources were also provided by the New

Horizons, Blue Sky, Green Prairies, and White Lagoon clusters at the CCRG-Rochester Institute of Technology, which were supported by NSF Grants No. PHY-0722703, No. DMS-0820923, No. AST-1028087, No. PHY-1229173, No. PHY-1726215, and No. PHY-2018420. This work used the ACCESS allocation TG-PHY060027N, founded by NSF, and project PHY20007 Frontera, an NSF-funded Petascale computing system at the Texas Advanced Computing Center (TACC).

[1] M. Campanelli, C. O. Lousto, Y. Zlochower, and D. Merritt, Astrophys. J. **659**, L5 (2007).
[2] J. A. González, M. D. Hannam, U. Sperhake, B. Brugmann, and S. Husa, Phys. Rev. Lett. **98**, 231101 (2007).
[3] S. Komossa, Adv. Astron. **2012**, 364973 (2012).
[4] M. Chiaberge, G. R. Tremblay, A. Capetti, and C. Norman, Astrophys. J. **861**, 56 (2018).
[5] M. Campanelli, C. O. Lousto, Y. Zlochower, and D. Merritt, Phys. Rev. Lett. **98**, 231102 (2007).
[6] C. O. Lousto and Y. Zlochower, Phys. Rev. Lett. **107**, 231102 (2011).
[7] M. Campanelli, C. O. Lousto, and Y. Zlochower, Phys. Rev. D **74**, 041501(R) (2006).
[8] V. Gayathri, J. Healy, J. Lange, B. O'Brien, M. Szczepanczyk, I. Bartos, M. Campanelli, S. Klimenko, C. O. Lousto, and R. O'Shaughnessy, Nat. Astron. **6**, 344 (2022).
[9] V. Cardoso *et al.*, Classical Quantum Gravity **29**, 244001 (2012).
[10] E. Berti, V. Cardoso, L. C. B. Crispino, L. Gualtieri, C. Herdeiro, and U. Sperhake, Int. J. Mod. Phys. D **25**, 1641022 (2016).
[11] V. Cardoso, L. Gualtieri, C. Herdeiro, and U. Sperhake, Living Rev. Relativity **18**, 1 (2015).
[12] G. Franciolini, A. Maharana, and F. Muia, Phys. Rev. D **106**, 103520 (2022).
[13] Q. Ding, Phys. Rev. D **104**, 043527 (2021).
[14] R.-G. Cai and S.-J. Wang, Phys. Rev. D **101**, 043508 (2020).
[15] S. W. Hawking, Phys. Rev. Lett. **26**, 1344 (1971).
[16] D. M. Eardley and S. B. Giddings, Phys. Rev. D **66**, 044011 (2002).
[17] M. Siino, Int. J. Mod. Phys. D **22**, 1350050 (2013).
[18] K. J. Mack, J. P. Ostriker, and M. Ricotti, Astrophys. J. **665**, 1277 (2007).
[19] L. Blecha and A. Loeb, Mon. Not. R. Astron. Soc. **390**, 1311 (2008).
[20] T. Harada and M. Kimura, Classical Quantum Gravity **31**, 243001 (2014).
[21] U. Sperhake, V. Cardoso, F. Pretorius, E. Berti, and J. A. Gonzalez, Phys. Rev. Lett. **101**, 161101 (2008).
[22] U. Sperhake, E. Berti, V. Cardoso, and F. Pretorius, Phys. Rev. Lett. **111**, 041101 (2013).
[23] J. Healy, I. Ruchlin, C. O. Lousto, and Y. Zlochower, Phys. Rev. D **94**, 104020 (2016).
[24] I. Ruchlin, J. Healy, C. O. Lousto, and Y. Zlochower, Phys. Rev. D **95**, 024033 (2017).
[25] M. Shibata, H. Okawa, and T. Yamamoto, Phys. Rev. D **78**, 101501(R) (2008).
[26] E. Berti, V. Cardoso, T. Hinderer, M. Lemos, F. Pretorius, U. Sperhake, and N. Yunes, Phys. Rev. D **81**, 104048 (2010).
[27] U. Sperhake, W. Cook, and D. Wang, Phys. Rev. D **100**, 104046 (2019).
[28] G. Bozzola, Phys. Rev. Lett. **128**, 071101 (2022).
[29] D. N. Page, Phys. Rev. D **107**, 064057 (2023).
[30] Y. Zlochower, J. G. Baker, M. Campanelli, and C. O. Lousto, Phys. Rev. D **72**, 024021 (2005).
[31] M. Campanelli, C. O. Lousto, P. Marronetti, and Y. Zlochower, Phys. Rev. Lett. **96**, 111101 (2006).
[32] T. Nakamura, K. Oohara, and Y. Kojima, Prog. Theor. Phys. Suppl. **90**, 1 (1987).
[33] M. Shibata and T. Nakamura, Phys. Rev. D **52**, 5428 (1995).
[34] T. W. Baumgarte and S. L. Shapiro, Phys. Rev. D **59**, 024007 (1998).
[35] Cactus Computational Toolkit home page, http://cactuscode.org.
[36] E. Schnetter, S. H. Hawley, and I. Hawke, Classical Quantum Gravity **21**, 1465 (2004).
[37] F. Löffler, J. Faber, E. Bentivegna, T. Bode, P. Diener, R. Haas, I. Hinder, B. C. Mundim, C. D. Ott, E. Schnetter, G. Allen, M. Campanelli, and P. Laguna, Classical Quantum Gravity **29**, 115001 (2012).
[38] Einstein Toolkit home page, http://einsteintoolkit.org.
[39] M. Ansorg, B. Brügmann, and W. Tichy, Phys. Rev. D **70**, 064011 (2004).
[40] J. Thornburg, Classical Quantum Gravity **21**, 743 (2004).
[41] M. Campanelli, C. O. Lousto, Y. Zlochower, B. Krishnan, and D. Merritt, Phys. Rev. D **75**, 064030 (2007).
[42] M. Campanelli and C. O. Lousto, Phys. Rev. D **59**, 124022 (1999).
[43] C. O. Lousto and Y. Zlochower, Phys. Rev. D **76**, 041502(R) (2007).
[44] H. Nakano, J. Healy, C. O. Lousto, and Y. Zlochower, Phys. Rev. D **91**, 104022 (2015).
[45] J. Healy, F. Herrmann, I. Hinder, D. M. Shoemaker, P. Laguna, and R. A. Matzner, Phys. Rev. Lett. **102**, 041101 (2009).
[46] U. Sperhake, E. Berti, V. Cardoso, F. Pretorius, and N. Yunes, Phys. Rev. D **83**, 024037 (2011).
[47] C. O. Lousto and Y. Zlochower, Phys. Rev. D **83**, 024003 (2011).
[48] A. Ciarfella, J. Healy, and C. O. Lousto (to be published).